

# GSVD-NMF: Recovering Missing Features in Non-negative Matrix Factorization

Youdong Guo, Timothy E. Holy

**Abstract**—Non-negative matrix factorization (NMF) is an important tool in signal processing and widely used to separate mixed sources into their components. However, NMF is NP-hard and thus may fail to discover the ideal factorization; moreover, the number of components may not be known in advance and thus features may be missed or incompletely separated. To recover missing components from under-complete NMF, we introduce GSVD-NMF, which proposes new components based on the generalized singular value decomposition (GSVD) between preliminary NMF results and the SVD of the original matrix. Simulation and experimental results demonstrate that GSVD-NMF often recovers missing features from under-complete NMF and helps NMF achieve better local optima.

**Index Terms**—Non-negative matrix factorization, GSVD, SVD, Feature recovery

## I. INTRODUCTION

Non-negative matrix factorization (NMF) is an effective tool for learning latent features from data in circumstances where plausible features are constrained to be nonnegative. It has been widely used in analysis of many types of data [1]–[10]. The NMF is given by

$$\mathbf{X} \approx \mathbf{W}\mathbf{H} \text{ subject to } \mathbf{W} \geq 0, \mathbf{H} \geq 0 \quad (1)$$

where  $\mathbf{W} \in \mathbb{R}^{m \times r_0}$  and  $\mathbf{H} \in \mathbb{R}^{r_0 \times n}$  are two non negative matrices.  $r_0$  is the number of components, which ideally represents the actual number of features in data matrix. To obtain  $\mathbf{W}$  and  $\mathbf{H}$  in Eq. (1), here we focus on minimizing the square-difference of the original matrix ( $\mathbf{X}$ ) and the factorization

$$D_E(\mathbf{X} \parallel \mathbf{W}\mathbf{H}) = \frac{1}{2} \|\mathbf{X} - \mathbf{W}\mathbf{H}\|_F^2 \quad (2)$$

This Squared Euclidean Distance is one of the most widely used objective functions for NMF.

Although NMF is widely used, in some circumstances it can fail to identify an accurate and comprehensive representation of the data features. Such failures arise from two sources. First, the exact number features in the data matrix is typically unknown and possibly undefined, so choosing  $r_0$  requires experimentation and judgement. If  $r_0$  is smaller than the number features in  $\mathbf{X}$ , the NMF would be “under-complete” with too few components in  $\mathbf{W}$  and  $\mathbf{H}$  to describe the independent features in  $\mathbf{X}$ . In such cases, features may be missed or integrated into other components. Various methods have been proposed to learn  $r_0$ , but no known procedure results

in an unambiguous answer [9], [11], [12]. Because performing NMF from scratch with a different number of components can be time-consuming, ideally one would have an efficient method to augment the components in a pre-existing solution.

Second, since NMF is not convex for  $\mathbf{W}$  and  $\mathbf{H}$  simultaneously, NMF may converge to local minimum or stop at saddle points. In this case, NMF would fail to give a good representation of features in  $\mathbf{X}$  even if the exact number  $r_0$  is known. Algorithms have been developed to mitigate this issue by focusing on special types of matrices for which the problem is convex [10], [13], improve initialization to increase the likelihood of landing in high-quality minima [14]–[19], and/or add regularization terms to the objective that steer optimization in desirable directions [20]–[24]. However, no algorithm can guarantee the global optimum in the general case.

Noting that SVD does find a globally-optimal matrix factorization, we propose to exploit the generalized singular value decomposition (GSVD) between existing NMF results and the SVD of  $\mathbf{X}$ . Directions with generalized singular value different from 1 correspond to discrepancies between the NMF and the SVD, and thus may present opportunities to improve the existing NMF. We introduce a convex (and thus deterministic) strategy to exploit the GSVD results to augment the NMF. The whole pipeline is tested by simulation and on multiple real-world datasets. The results demonstrate that our method can help recover features missed by under-complete standard NMF. Moreover, starting from under-complete NMF (deliberately setting rank number smaller than the number of features in  $\mathbf{X}$ ), the proposed method can help NMF converge to better local optima. Finally, the proposed method allows the incremental expansion of the number of components, which can be convenient and effective for interactive analysis of large-scale data.

## II. METHOD

The whole pipeline of the proposed method is given in Fig (1). Given that standard NMF typically yields local optima and SVD constitutes a global optimum of matrix factorization, our core concept involves identifying features captured by SVD but absent in NMF outcomes. These identified features are then incorporated as new components into the existing NMF results.  $\mathbf{W}_0$  and  $\mathbf{H}_0$  are the results of under-complete NMF with  $r_0$  components. We use  $\mathbf{U}_{r_0}$ ,  $\mathbf{\Sigma}_{r_0}$  and  $\mathbf{V}_{r_0}$  to denote the results of rank- $r_0$  approximate SVD, which is the global optimum of rank- $r_0$  matrix factorization of  $\mathbf{X}$ . Using the GSVD, we compare the results of under-complete NMF and rank- $r_0$  SVD, and on that basis propose new rows (denoted

Youdong Guo is with the Department of Neuroscience, Washington University in St. Louis, St. Louis, MO, 63130, USA

Timothy E. Holy is with the Departments of Neuroscience and Biomedical Engineering, Washington University in St. Louis, St. Louis, MO, 63130, USA (email: holy@wustl.edu)

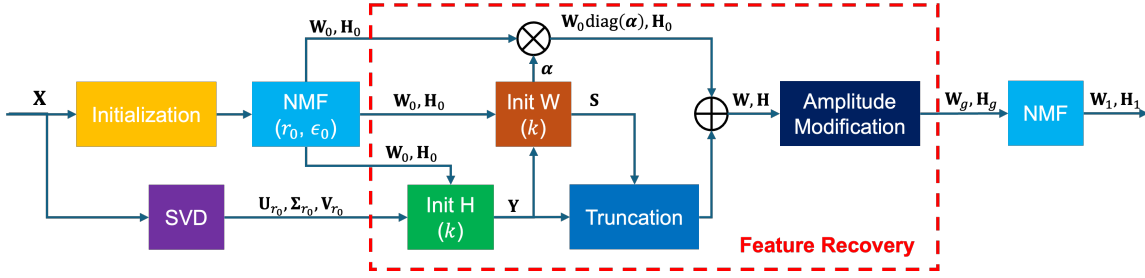


Fig. 1. The whole pipeline of GSVD-based feature recovery with 2 stage NMF

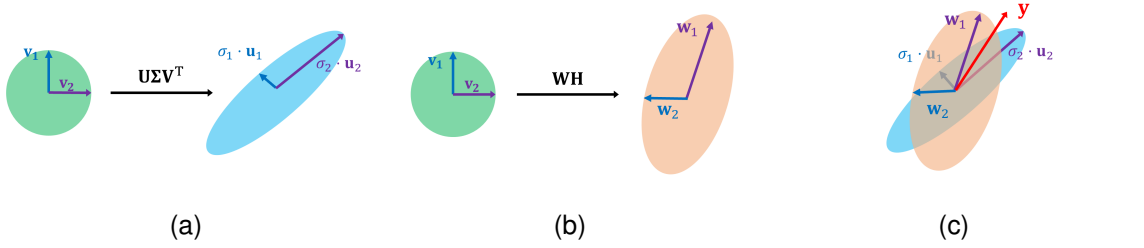


Fig. 2. Illustration of GSVD-based feature recovery for NMF. (a) The SVD ellipse picture for a matrix. (b) The NMF ellipse picture for a matrix. (c) The new direction found by GSVD-based method for intermediate over-complete NMF initialization.

$\mathbf{Y}$ ) for  $\mathbf{H}$  and new columns (denoted  $\mathbf{S}$ ) for  $\mathbf{W}$ .  $\mathbf{S}$  and  $\mathbf{Y}$  are not guaranteed to be nonnegative, so these are truncated and the amplitude of old and new components are adjusted together by least-squares. Finally, all components are polished by NMF to produce the final factorization. We now describe these steps in detail.

Our concept is most easily understood by viewing matrices as linear transformations that act on vectors in the domain space, which in Fig 2 will be represented as points in the unit disc (green). Fig 2(a) represents the action of the SVD of  $\mathbf{X}$  on a unit disc and Fig 2(b) is action of the NMF of  $\mathbf{X}$  on the unit disc, projected into the subspace spanned by the SVD. Any difference between the resulting ellipses in the range-space (Fig 2(c)) represents a mismatch between the NMF and the optimal rank- $r_0$  factorization. Our primary objective is to identify new directions that can reshape the NMF solution to more closely approximate the SVD solution, as exemplified by the vector  $\mathbf{y}$  in Fig 2(c).

Naively, one might imagine that the new direction  $\mathbf{y} \in \mathbb{R}^{n \times 1}$  could be obtained by optimizing

$$\max_{\mathbf{y}} \frac{\|\mathbf{U}_{r_0} \Sigma_{r_0} \mathbf{V}_{r_0}^T \mathbf{y}\|^2}{\|\mathbf{W}_0 \mathbf{H}_0 \mathbf{y}\|^2} \quad (3)$$

However, this suffers from a conceptual problem: (3) is infinite for any  $\mathbf{y}$  in the null space of  $\mathbf{W}_0 \mathbf{H}_0$  but not in the null space of the SVD. As there are at least  $\min(m, n) - r_0$  dimensions in the nullspace of  $\mathbf{W}_0 \mathbf{H}_0$ , any discrepancy between the SVD and NMF range subspaces provides an infinite number of potential solutions for (3). Thus, we instead optimize a variant of (3) that projects the NMF result down to the SVD subspace:

$$\max_{\hat{\mathbf{y}}} \frac{\|\Sigma_{r_0} \hat{\mathbf{y}}\|^2}{\|\mathbf{U}_{r_0}^T \mathbf{W}_0 \mathbf{H}_0 \mathbf{V}_{r_0} \hat{\mathbf{y}}\|^2} \quad (4)$$

where  $\hat{\mathbf{y}} \in \mathbb{R}^{r_0 \times 1}$ . To solve this problem, let

$\lambda = \frac{\|\Sigma_{r_0} \hat{\mathbf{y}}\|^2 / \|\mathbf{U}_{r_0}^T \mathbf{W}_0 \mathbf{H}_0 \mathbf{V}_{r_0} \hat{\mathbf{y}}\|^2}{\|\mathbf{U}_{r_0}^T \mathbf{W}_0 \mathbf{H}_0 \mathbf{V}_{r_0} \hat{\mathbf{y}}\|^2}$  and multiply by  $\|\mathbf{U}_{r_0}^T \mathbf{W}_0 \mathbf{H}_0 \mathbf{V}_{r_0} \hat{\mathbf{y}}\|^2$  on both sides, yielding

$$\lambda \|\mathbf{U}_{r_0}^T \mathbf{B} \mathbf{V}_{r_0} \hat{\mathbf{y}}\|^2 = \|\Sigma_{r_0} \hat{\mathbf{y}}\|^2 \quad (5)$$

where  $\mathbf{B} = \mathbf{W}_0 \mathbf{H}_0$ . Computing the derivative with respect to  $\hat{\mathbf{y}}$  and setting  $\partial \lambda / \partial \hat{\mathbf{y}} = 0$  gives

$$\Sigma_{r_0}^T \Sigma_{r_0} \hat{\mathbf{y}} = \lambda \mathbf{V}_{r_0}^T \mathbf{B}^T \mathbf{U}_{r_0} \mathbf{U}_{r_0}^T \mathbf{B} \mathbf{V}_{r_0} \hat{\mathbf{y}} \quad (6)$$

This problem can be solved by the GSVD of  $\Sigma_{r_0}$  and  $\mathbf{U}_{r_0}^T \mathbf{B} \mathbf{V}_{r_0}$ , resulting in

$$\begin{aligned} \Sigma_{r_0} &= \mathbf{M}_1 \mathbf{D}_1 \mathbf{Q}^T \\ \mathbf{U}_{r_0}^T \mathbf{B} \mathbf{V}_{r_0} &= \mathbf{M}_2 \mathbf{D}_2 \mathbf{Q}^T \end{aligned} \quad (7)$$

The matrices  $\mathbf{M}_1, \mathbf{M}_2 \in \mathbb{R}^{r_0 \times r_0}$  are unitary and  $\mathbf{Q} \in \mathbb{R}^{r_0 \times r_0}$ . Here, the matrices  $\mathbf{D}_1, \mathbf{D}_2 \in \mathbb{R}^{r_0 \times r_0}$  are given by

$$\mathbf{D}_1 = \begin{pmatrix} \mathbf{I} & \mathbf{0} \\ \mathbf{0} & \mathbf{C} \end{pmatrix}, \quad \mathbf{D}_2 = \begin{pmatrix} \mathbf{0} & \mathbf{G} \\ \mathbf{0} & \mathbf{0} \end{pmatrix} \quad (8)$$

where  $\mathbf{C}, \mathbf{G} \in \mathbb{R}^{l \times l}$  are real, diagonal matrices and  $l$  denotes the rank of  $\mathbf{U}_{r_0}^T \mathbf{B} \mathbf{V}_{r_0}$ .  $\mathbf{I} \in \mathbb{R}^{(r_0-l) \times (r_0-l)}$  is identity matrix. If  $l = r_0$ ,  $\mathbf{D}_1 = \mathbf{C}$  and  $\mathbf{D}_2 = \mathbf{G}$ . Plugging (7) into (6) yields

$$\mathbf{D}_1^T \mathbf{D}_1 \mathbf{Q}^T \hat{\mathbf{y}} = \lambda \mathbf{D}_2^T \mathbf{D}_2 \mathbf{Q}^T \hat{\mathbf{y}} \quad (9)$$

Letting  $\mathbf{z} = \mathbf{Q}^T \hat{\mathbf{y}}$ , we need to solve

$$\mathbf{D}_1^T \mathbf{D}_1 \mathbf{z} = \lambda \mathbf{D}_2^T \mathbf{D}_2 \mathbf{z} \quad (10)$$

$\mathbf{D}_1^T \mathbf{D}_1$  and  $\mathbf{D}_2^T \mathbf{D}_2$  are real, non-negative diagonal matrices. Assume that  $\mathbf{D}_1^T \mathbf{D}_1 = \text{diag}(d_{11}^2, \dots, d_{1r_0}^2)$  and  $\mathbf{D}_2^T \mathbf{D}_2 = \text{diag}(d_{21}^2, \dots, d_{2r_0}^2)$ , the generalized singular value  $d_{1i}/d_{2i}$  are infinite for  $i = 1, \dots, r_0 - l$ , and are finite for the remaining  $l$  values. If the rank of  $\mathbf{B}$  is  $r_0$  ( $l = r_0$ ), all generalized singular values are finite. When  $d_{1i}/d_{2i}$  is finite ( $d_{2i} \neq 0$ ),

the corresponding  $\mathbf{z}_i$  are the unit coordinate vectors. Thus,  $\hat{\mathbf{y}}_i = (\mathbf{Q}^T)^{-1} \mathbf{z}_i$  and the new directions are given by

$$\mathbf{y}_i = \mathbf{V}_{r_0} (\mathbf{Q}^T)^{-1} \mathbf{z}_i \quad (11)$$

$\mathbf{y}_i$  is the  $i$ -th column of  $\mathbf{V}_{r_0} (\mathbf{Q}^T)^{-1}$  for  $i = r_0 - l + 1, \dots, r_0$ . When  $i = 1, \dots, r_0 - l$ ,  $d_{1i}/d_{2i}$  is infinite ( $d_{2i} = 0$ ), we similarly select  $\mathbf{y}_i$  using the  $i$ -th column of  $\mathbf{V}_{r_0} (\mathbf{Q}^T)^{-1}$ . These represent directions that are missing entirely from the  $\mathbf{W}_0 \mathbf{H}_0$  factorization.

We expect that GSVD-NMF has the capacity to suggest missing directions only for rank-2 NMF and higher. For rank-1 factorizations, NMF algorithms find the global optimum, and since the first component in the SVD of a non-negative matrix is non-negative, the rank-1 NMF solution should already be equivalent to the first SVD component.

After fixing  $\mathbf{Y}$ , the corresponding additional components for  $\mathbf{W}_0$  (defined as  $\mathbf{S}$ ) are derived from a least-squares problem

$$\min_{\mathbf{S}, \boldsymbol{\alpha}} \|\mathbf{X} - \sum_{p=1}^{r_0} \alpha_p \mathbf{w}_{0p} \mathbf{h}_{0p}^T - \mathbf{S} \mathbf{Y}\|^2 \quad (12)$$

where  $\mathbf{w}_{0p}$  is the  $p$ -th column in  $\mathbf{W}_0$ ,  $\mathbf{h}_{0p}$  is the  $p$ -th row in  $\mathbf{H}_0$  and  $\boldsymbol{\alpha} = [\alpha_1, \alpha_2, \dots, \alpha_{r_0}]$ . Here  $\boldsymbol{\alpha}$  is required to be non-negative in order to preserve the non-negativity of the original components  $\mathbf{W}_0 \mathbf{H}_0$ . The vector  $\boldsymbol{\alpha}$  is introduced to modulate the magnitude of the components within  $\mathbf{W}_0$  thereby augmenting the adaptability of the matrix  $\mathbf{S}$  in the minimization of (12). (12) can be expanded to the quadratic form

$$\begin{aligned} E &= \|\mathbf{X} - \sum_{p=1}^{r_0} \alpha_p \mathbf{w}_{0p} \mathbf{h}_{0p}^T - \mathbf{S} \mathbf{Y}\|^2 \\ &= \boldsymbol{\alpha}^T \boldsymbol{\Theta} \boldsymbol{\alpha} - 2 \boldsymbol{\xi}^T \boldsymbol{\alpha} + \Phi - 2 \boldsymbol{\gamma}^T \mathbf{m} \\ &\quad + 2 \boldsymbol{\alpha}^T \mathbf{P} \mathbf{m} + \mathbf{m}^T \boldsymbol{\Psi} \mathbf{m} \end{aligned} \quad (13)$$

where  $\mathbf{m} = [\mathbf{s}_1^T, \mathbf{s}_2^T, \dots, \mathbf{s}_k^T]^T$  represents  $\mathbf{S}$  as a long vector,  $\boldsymbol{\Theta} \in \mathbb{R}^{r_0 \times r_0}$  with  $\boldsymbol{\Theta} = (\mathbf{W}_0^T \mathbf{W}_0) \circ (\mathbf{H}_0 \mathbf{H}_0^T)$ ,  $\boldsymbol{\xi} \in \mathbb{R}^{r_0 \times 1}$  with  $\xi_p = \mathbf{w}_{0p}^T \mathbf{X} \mathbf{h}_{0p}$ ,  $\Phi = \sum_{i,j} X_{ij}$ ,  $\boldsymbol{\gamma} = [(\mathbf{X} \mathbf{y}_1)^T, (\mathbf{X} \mathbf{y}_2)^T, \dots, (\mathbf{X} \mathbf{y}_k)^T]^T$ .  $\mathbf{P}$  and  $\boldsymbol{\Psi}$  are a block matrices, where  $\mathbf{P}_{pp'} = \mathbf{h}_{0p}^T \mathbf{y}_{p'} \mathbf{w}_{0p}^T$  and  $\boldsymbol{\Psi}_{pp'} = \mathbf{y}_{p'}^T \mathbf{y}_p \mathbf{I}_m$ ,  $\mathbf{I}_m \in \mathbb{R}^{m \times m}$  is an identity matrix. The stationary point of  $E$  with respect to  $\mathbf{m}$  is

$$\mathbf{m} = \boldsymbol{\Psi}^{-1} (\boldsymbol{\gamma} - \mathbf{P}^T \boldsymbol{\alpha}) \quad (14)$$

Substituting (14) into (12) yields

$$\begin{aligned} E &= \boldsymbol{\alpha}^T (\boldsymbol{\Theta} - \mathbf{P} \boldsymbol{\Psi}^{-1} \mathbf{P}^T) \boldsymbol{\alpha} \\ &\quad - 2 \left( \boldsymbol{\xi}^T - \boldsymbol{\gamma}^T \boldsymbol{\Psi}^{-1} \mathbf{P}^T \right) \boldsymbol{\alpha} + \Phi - \boldsymbol{\gamma}^T \boldsymbol{\Psi}^{-1} \boldsymbol{\gamma} \end{aligned} \quad (15)$$

Since (15) is derived from the non-negative least square problem (13), the quadratic in (15) must be positive semidefinite, and thus this problem is convex and admits a deterministic solution [25], [26].

To impose non-negativity constraints on  $\mathbf{S}$  and  $\mathbf{Y}$  from (14) and (15) without significantly increasing the computational demand, we use the truncation step of NNDSVD [14]. Since the truncation alters the entries in  $\mathbf{S}$  and  $\mathbf{Y}$ , we let  $\mathbf{W} =$

$[\mathbf{W}_0 \text{diag}(\boldsymbol{\alpha}) \mathbf{W}_{\text{new}}]$  and  $\mathbf{H} = [\mathbf{H}_0; \mathbf{H}_{\text{new}}]$ , all components in  $\mathbf{W}$  and  $\mathbf{H}$  are re-optimized together by

$$\min_{\boldsymbol{\beta} \geq 0} \|\mathbf{X} - \sum_{p=1}^{r_0+k} \beta_p \mathbf{w}_p \mathbf{h}_p^T\|^2 \quad (16)$$

where  $\boldsymbol{\beta} = [\beta_1, \beta_2, \dots, \beta_{r_0+k}]$ .  $\mathbf{w}_p, \mathbf{h}_p$  are the  $p$ -th column and  $p$ -th row in  $\mathbf{W}, \mathbf{H}$  respectively. (16) is also a nonnegative least squares problem and thus convex. The final step is refinement via NMF, initialized with  $\mathbf{W}_g = \mathbf{W} \text{diag}(\boldsymbol{\beta})$  and  $\mathbf{H}_g = \mathbf{H}$ . The GSVD-based feature recovery is summarized in Algorithm 1.

---

#### Algorithm 1 GSVD-based feature recovery

---

**Input:**  $\mathbf{W}_0, \mathbf{H}_0, \mathbf{U}_{r_0}, \boldsymbol{\Sigma}_{r_0}, \mathbf{V}_{r_0}, k$

**Output:**  $\mathbf{W}_g, \mathbf{H}_g$

Compute  $\mathbf{Q}, \mathbf{C}, \mathbf{G}, \mathbf{D}_1, \mathbf{D}_2$  by solving (7) and (8)

$l \leftarrow \text{size}(\mathbf{G}, 1)$

$\boldsymbol{\lambda} \leftarrow \text{vcat} \left( \text{fill}(\text{Inf}, r_0 - l), \text{diag} \left( (\mathbf{G}^T \mathbf{G})^{-1} \mathbf{C}^T \mathbf{C} \right) \right)$

$\mathbf{Y} \leftarrow k$  columns in  $\mathbf{V}_{r_0} (\mathbf{Q}^T)^{-1}$  corresponding to the largest  $k$  values in  $\boldsymbol{\lambda}$

Compute  $\mathbf{S}, \boldsymbol{\alpha}$  with (15)

Compute  $\mathbf{W}_{\text{new}}, \mathbf{H}_{\text{new}}$  by truncating  $\mathbf{S}, \mathbf{Y}$  (Truncation step in NNDSVD)

$\mathbf{W} \leftarrow [\mathbf{W}_0 \text{diag}(\boldsymbol{\alpha}) \mathbf{W}_{\text{new}}]$

$\mathbf{H} \leftarrow [\mathbf{H}_0; \mathbf{Y}_+]$

Compute  $\boldsymbol{\beta}$  with (16)

$\mathbf{W}_g \leftarrow \mathbf{W} \text{diag}(\boldsymbol{\beta})$

$\mathbf{H}_g \leftarrow \mathbf{H}$

---

If the SVD in (4) has more components than the NMF, it is guaranteed that some singular values  $\lambda$  will be infinite, and our strategy will first select directions missing from the NMF. When adopting this strategy, the schematic in Fig 2 depicting the polishing of existing directions is no longer relevant.

### III. SIMULATION AND EXPERIMENTAL RESULTS

In this section, we demonstrate the effectiveness of GSVD-NMF and compare its performance with standard NMF on synthetic and real-world data. The simulation and experiments were performed using Julia 1.10 on Washington University in St. Louis RIS scientific computing platform with Intel\_Xeon\_Gold6242CPU280GHz 8G RAM. The NMF algorithm chosen for comparison and refinement in the GSVD-NMF pipeline Hierarchical alternating least squares (HALS) [27], one of the most accurate and widely-used NMF algorithms [11], [28]. To determine convergence, here we monitor the maximum relative change in the Frobenius norm of the columns of  $\mathbf{W} \in \mathbb{R}^{m \times r}$  and the rows of  $\mathbf{H} \in \mathbb{R}^{r \times n}$  (given in (17)), and stop iterating when

$$\begin{aligned} \|\mathbf{w}_j^{(k+1)} - \mathbf{w}_j^{(k)}\|^2 &\leq \epsilon \|\mathbf{w}_j^{(k+1)} + \mathbf{w}_j^{(k)}\|^2 \\ \|\mathbf{h}_j^{(k+1)} - \mathbf{h}_j^{(k)}\|^2 &\leq \epsilon \|\mathbf{h}_j^{(k+1)} + \mathbf{h}_j^{(k)}\|^2 \end{aligned} \quad (17)$$

for  $j = 1, 2, \dots, r$ , for some choice of  $\epsilon$ . In these expressions,  $\mathbf{w}_j$  and  $\mathbf{h}_j$  are the  $j$ -th column and  $j$ -th row in  $\mathbf{W}$  and  $\mathbf{H}$

respectively. Unless otherwise specified,  $\epsilon = 10^{-4}$  was used. The relative fitting error between  $\mathbf{WH}$  and the input matrix  $\mathbf{X}$ ,  $100\|\mathbf{X} - \mathbf{WH}\|_2^2 / \|\mathbf{X}\|_2^2$ , was used to evaluate the local optima of NMF. This measures how well the factorization fit the input matrix.

### A. Synthetic data: an illustrative example

By identifying new directions from the SVD, GSVD-NMF has the potential to recover missing components from under-complete NMF results. To assess this, we first tested GSVD-NMF on synthetic data with 10 ground truth components, which are shown in figure 3(a). Running HALS with 10 components (initialized with NNDSVD) yielded an inaccurate solution, shown in figure 3(b).

To exploit GSVD-NMF, we started from the solution returned by HALS with 9 components, one less than the number of ground truth components, obtaining the result shown in figure 3(c). One sees that two components of the ground truth are blended, figure 3(c). To test for missing information, we compared the 9-component NMF with a 9-component SVD using GSVD as described in Sec. II. This identified a “missing” direction relate to the first (large-magnitude) generalized eigenvalue, Figure 3(d). Note that this analysis provides support for only one additional component. The component recovered by the feature recovery step in the pipeline (figure 1) is shown in green in figure 3(e). After optimizing this 10-component “re-initialization” using HALS, the final NMF result, shown in figure 3 (f), accurately represents each ground truth component. Therefore, GSVD-NMF can recover the missing component from under-complete NMF, and in this case performs better than naive HALS even when the correct number of components is known.

### B. Experimental results

1) *Data sets*: We also tested the performance of GSVD-NMF on four real-world datasets, which includes two liquid chromatography-mass spectrometry datasets (LCMS1 and LCMS2, shown in figure 4(a) and (b), doi:10.25345/C58C9R77T), and two audio datasets. The audio datasets feature the first measure of “Mary had a little lamb” and the first 30 seconds of “Prelude and Fugue No.1 in C major” by J.S. Bach, played by Glenn Gould, both of which are taken from reference [7]. Figure 4(c) and (d) illustrates the amplitude spectrograms of audio data. Details about all four real-world datasets are presented in Table I and the column  $r$  lists the “real” number of features we selected for this paper.

2) *Method of comparison*: Since the ground truth components of real-world data are undetermined, we assessed methods in terms of the value of the objective, Eq. 2, with smaller values indicating better solutions. For each random initialization, we compared the local optima obtained by GSVD-NMF and standard NMF. Standard NMF was initialized with a random rank- $r$  solution, with  $r$  given in Table I. GSVD-NMF was initialized with the first  $r_0 = r - 1$  components of this same initialization, and then a single new component was added by GSVD-NMF to achieve rank  $r$ ; thus, the two

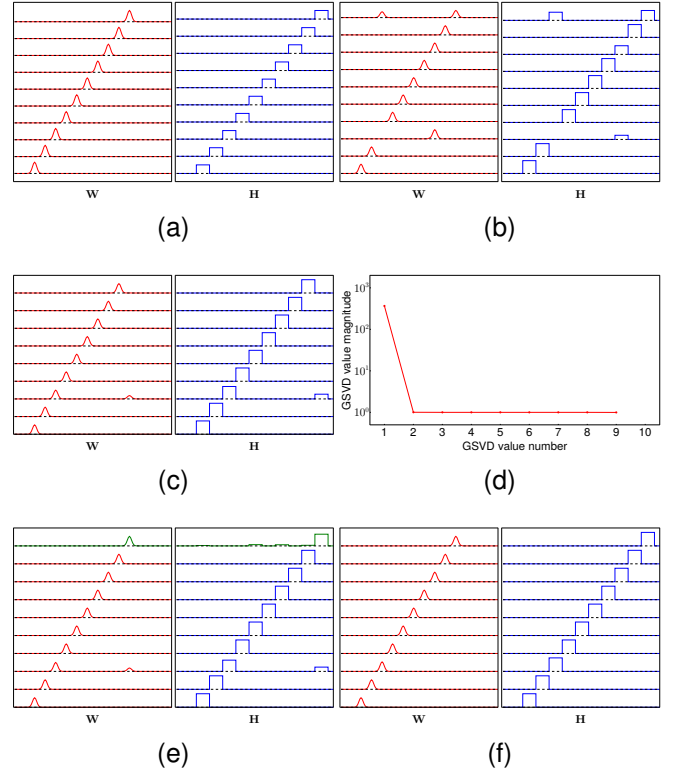


Fig. 3. A synthetic example used to illustrate the GSVD-NMF for feature recovery ( $k = 1$ ), displaying  $\mathbf{W}$  and  $\mathbf{H}$ . (a) Ground truth of  $\mathbf{W}$  and  $\mathbf{H}$  (10 features). (b) Standard NMF results initialized with NNDSVD. Despite knowing the correct number of components, two features are incompletely separated. (c) Standard NMF results with 9 components. (d) The generalized singular value spectrum. (e) Feature recovery results ( $\mathbf{W}_g, \mathbf{H}_g$ ). (f) Final NMF results ( $\mathbf{W}_1, \mathbf{H}_1$ ).

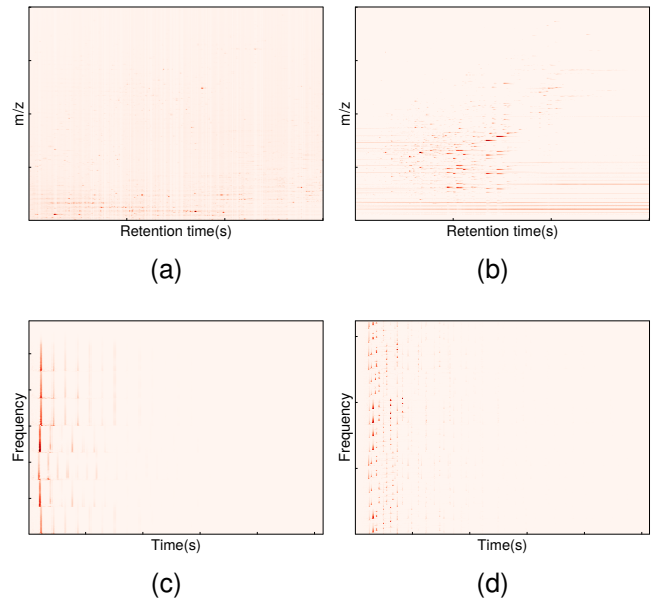


Fig. 4. (a) LCMS1. (b) LCMS2. (c) The amplitude spectrogram of “Mary had a little lamb”. (d) The amplitude spectrogram of “Prelude and Fugue No.1 in C major”

solutions start from as much of a shared initialization as can be achieved given their differences in initial rank. Solution

TABLE I  
DESCRIPTION OF DATA SETS

| No. | Data sets                                    | Size             | $r$ |
|-----|--|------------------|-----|
| 1   | LCMS1  | $400 \times 600$ | 17  |
| 2   | LCMS2  | $400 \times 600$ | 23  |
| 3   | Mary had a little lamb (MHLL)                | $257 \times 294$ | 3   |
| 4   | Prelude and Fugue No.1 in C major (P&F No.1) | $513 \times 647$ | 13  |

TABLE II  
GSVD-NMF VS STANDARD NMF WITH DIFFERENT INITIALIZATION

|          | Fitting error (%) : Standard NMF / GSVD-NMF |                    |             |             |
|----------|---|--------------------|-------------|-------------|
|          | LCMS1                                       | LCMS2              | MHLL        | P&F No.1    |
| NNDSVD   | 3.97 / 3.97                                 | <b>4.05 / 3.99</b> | 3.08 / 3.08 | 2.85 / 3.12 |
| NNDSVDa  | 3.97 / 3.96                                 | <b>4.07 / 4.01</b> | 3.08 / 3.08 | 2.85 / 3.12 |
| NNDSVDar | 3.97 / 3.96                                 | <b>4.05 / 3.99</b> | 3.08 / 3.08 | 2.85 / 3.12 |

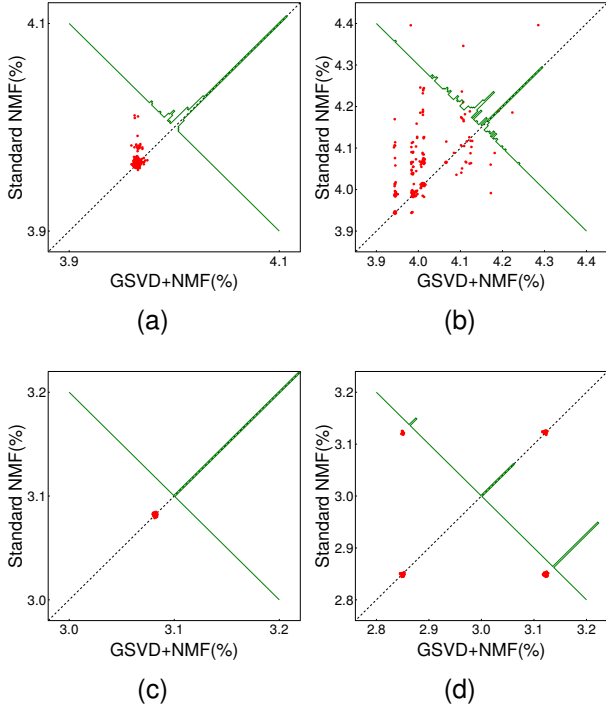


Fig. 5. Comparing the fitting error of standard NMF and GSVD-NMF. (a) LCMS1. (b) LCMS2. (c) Mary had a little lamb. (d) Prelude and Fugue No.1 in C major.

objective values are compared in scatter plots, where each dot represents a single random initialization, and green lines represent the histogram of perpendicular distances between points and the diagonal (a.k.a., equal performance) in the figure.

3) *GSVD-NMF converges to better local optima*: The comparison of local optima achieved by standard NMF and GSVD-NMF is given in figure 5. The horizontal axis denotes the relative fitting error of final results of GSVD-NMF while the vertical axis represents that of standard NMF.

Figure 5 demonstrates that NMF converges to multiple local optima for both LCMS data sets. For the melody “Mary had a little lamb”, there is only one local optimum detected. For “Prelude and Fugue No.1 in C major”, two local optima are identified. In aggregate, most of the points in 5 are above or along the diagonal line, indicating that GSVD-NMF either matches or improves the convergence of NMF in the majority of cases, particularly for the LCMS data. However, there are cases (5d) where standard NMF more frequently converges to the better solution.

We also evaluated the performance of GSVD-NMF using deterministic initialization methods like NNDSVD, NNDSVDa, and NNDSVDar [14], with the results shown in Table II. GSVD-NMF performed comparably or better than standard NMF across three datasets. However, on “Prelude and Fugue No.1 in C major”, standard NMF outperforms GSVD-NMF, similar to the results in figure 5(d). This outcome demonstrates the perhaps-surprising point that GSVD-NMF can improve NMF even when the very same components of the SVD have already been used to initialize NMF.

4) *The choice of  $\epsilon_0$* : GSVD-NMF runs standard NMF twice: the initial under-complete NMF and the final NMF (figure 1). So far, all our results have employed the same  $\epsilon = 10^{-4}$  in (17) for all NMF runs. One might wonder whether both need to be run to convergence, or whether for computational efficiency one might be able to terminate under-complete NMF early to save computation time.

The effects of reducing the stringency of the under-complete NMF ( $\epsilon_0$ ) steps are shown in figure 6. The tolerance has little effect on “Mary had a little lamb” and the “Prelude and Fugue No.1 in C major” datasets, although for the latter we note that the diagonal tends to be more highly favored at  $\epsilon_0 = 0.1$ . On both LCMS data sets, the advantages of GSVD-NMF grow with the stringency of  $\epsilon_0$ . Overall, these results demonstrate that in GSVD-NMF, the under-complete NMF can be run at higher tolerance (lower stringency) but with higher risk of landing in worse local optima. However, at all tested stringencies GSVD-NMF outperforms standard NMF in aggregate.

5) *The choice of  $k$* : It should be noted that the all of above experiments set  $k = 1$ , a systematic procedure that appears to be broadly successful. In practice, we may wish to add multiple components simultaneously, rather than iteratively adding one component at a time, to make the whole pipeline more efficient. Thus, it is valuable to investigate the role of  $k$  on final results.

To investigate how this parameter affects the final result, the experiment in Sec. III-B3 (200 random initialized trials) was conducted with different  $k$ . Figure 7 illustrates the difference between the fitting error of standard NMF and that of GSVD-NMF. Consistent with the results in figure 5, GSVD-NMF finds superior local optimum in most cases on both LCMS data sets regardless of  $k$ . On “Prelude and Fugue No.1 in C major,” we see that GSVD-NMF’s worse performance is restricted to the  $k = 1$  case; for any larger  $k$ , the solution is similar to that of standard NMF. In real practice, the choice of  $k$  can be guided by the eigenvalue spectrum (Figure 3d), but in general we recommend sticking to fairly small values

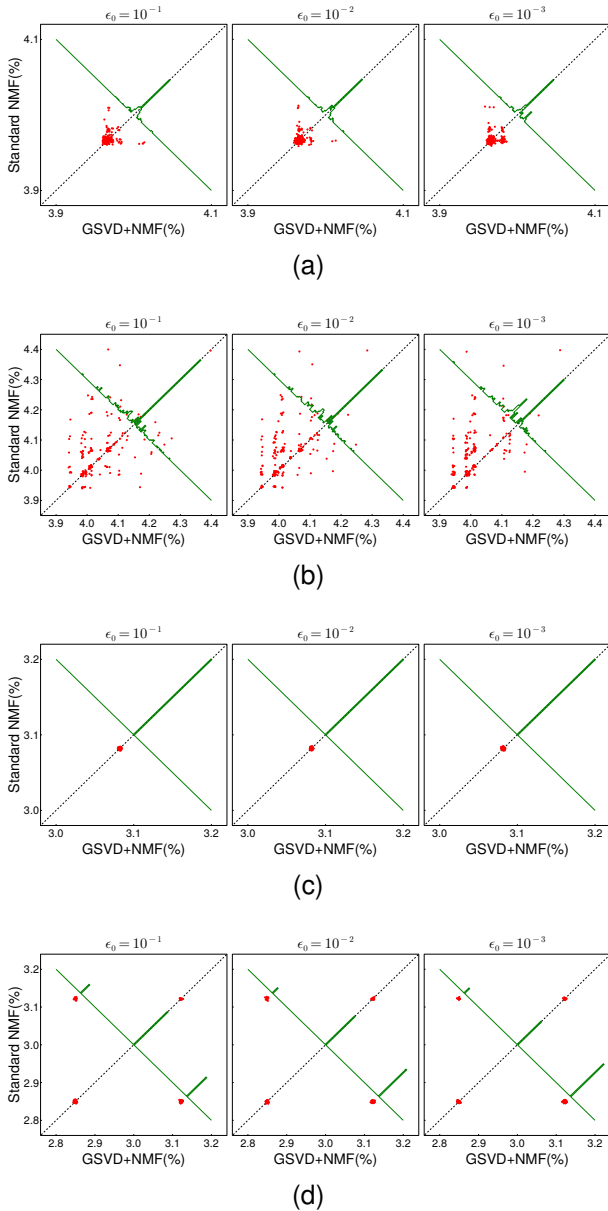


Fig. 6. The effect of convergence tolerance  $\epsilon_0$  on final results of GSVD-NMF. Panels should be compared to those of figure 5, which used  $\epsilon_0 = 10^{-4}$ . (a) LCMS1. (b) LCMS2. (c) Mary had a little lamb. (d) Prelude and Fugue No.1 in C major.

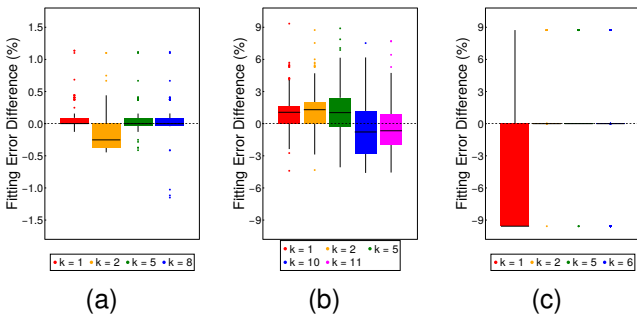


Fig. 7. The effect of different  $k$ : (a) LCMS1. (b) LCMS2. (c) Prelude and Fugue No.1 in C major.

of  $k$ .

## IV. CONCLUSION

In conclusion, we propose a new strategy to reconstruct missing components from under-complete or poor local NMF solutions. Our strategy exploits the generalized SVD between the initial NMF solution and the SVD of the same rank to identify “missing features” and suggest new component(s), which are then refined by another round of NMF. We show that GSVD-NMF is capable of iteratively recovering missing components for under-complete NMF, enabling a strategy in which one incrementally grows the rank of an NMF solution without the need to start from scratch. This may have practical benefits in real applications, particularly for large data sets, when the number of components is not known. Even when compared against NMF of the same rank, GSVD-NMF often outperformed standard NMF in terms of the quality of its local optima.

The code for this paper is available at <https://github.com/HolyLab/GsvdInitialization.jl.git>

## ACKNOWLEDGMENTS

This work was supported by NIH grants R01DC020034 and R01DC010381 (T.E.H.).

## REFERENCES

- [1] D. D. Lee and H. S. Seung, “Learning the parts of objects by non-negative matrix factorization,” *nature*, vol. 401, no. 6755, pp. 788–791, 1999.
- [2] R. Rajabi and H. Ghassemian, “Spectral unmixing of hyperspectral imagery using multilayer nmf,” *IEEE Geoscience and Remote Sensing Letters*, vol. 12, no. 1, pp. 38–42, 2014.
- [3] W. Wang, Y. Qian, and Y. Y. Tang, “Hypergraph-regularized sparse nmf for hyperspectral unmixing,” *IEEE journal of selected topics in applied earth observations and remote sensing*, vol. 9, no. 2, pp. 681–694, 2016.
- [4] Y. Chen, H. Zhang, R. Liu, Z. Ye, and J. Lin, “Experimental explorations on short text topic mining between lda and nmf based schemes,” *Knowledge-Based Systems*, vol. 163, pp. 1–13, 2019.
- [5] K. Kowsari, K. Jafari Meimandi, M. Heidarysafa, S. Mendu, L. Barnes, and D. Brown, “Text classification algorithms: A survey,” *Information*, vol. 10, no. 4, p. 150, 2019.
- [6] J. F. Gemmeke, L. Vuegen, P. Karsmakers, B. Vanrumste *et al.*, “An exemplar-based nmf approach to audio event detection,” in *2013 IEEE workshop on applications of signal processing to audio and acoustics*. IEEE, 2013, pp. 1–4.
- [7] V. Leplat, N. Gillis, and A. M. Ang, “Blind audio source separation with minimum-volume beta-divergence nmf,” *IEEE Transactions on Signal Processing*, vol. 68, pp. 3400–3410, 2020.
- [8] R. Dubroca, C. Junor, and A. Souloumiac, “Weighted nmf for high-resolution mass spectrometry analysis,” in *2012 Proceedings of the 20th European Signal Processing Conference (EUSIPCO)*. IEEE, 2012, pp. 1806–1810.
- [9] X. Lin and P. C. Boutros, “Optimization and expansion of non-negative matrix factorization,” *BMC bioinformatics*, vol. 21, no. 1, p. 7, 2020.
- [10] P. McClure, F. Khalifa, A. Soliman, M. Abou El-Ghar, G. Gimelfarb, A. Elmagraby, and A. El-Baz, “A novel nmf guided level-set for dwi prostate segmentation,” *Journal of Computer Science & Systems Biology*, vol. 7, no. 6, p. 1, 2014.
- [11] N. Gillis, “The why and how of nonnegative matrix factorization,” *Regularization, optimization, kernels, and support vector machines*, vol. 12, no. 257, pp. 257–291, 2014.
- [12] P. Fogel, C. Geissler, N. Morizet, and G. Luta, “On rank selection in non-negative matrix factorization using concordance,” *Mathematics*, vol. 11, no. 22, p. 4611, 2023.
- [13] S. Arora, R. Ge, R. Kannan, and A. Moitra, “Computing a nonnegative matrix factorization—provably,” in *Proceedings of the forty-fourth annual ACM symposium on Theory of computing*, 2012, pp. 145–162.
- [14] C. Boutsidis and E. Gallopoulos, “Svd based initialization: A head start for nonnegative matrix factorization,” *Pattern recognition*, vol. 41, no. 4, pp. 1350–1362, 2008.

- [15] F. Esposito, "A review on initialization methods for nonnegative matrix factorization: towards omics data experiments," *Mathematics*, vol. 9, no. 9, p. 1006, 2021.
- [16] S. Fathi Hafshejani and Z. Moaberfard, "Initialization for non-negative matrix factorization: a comprehensive review," *International Journal of Data Science and Analytics*, vol. 16, no. 1, pp. 119–134, 2023.
- [17] G. Casalino, N. Del Buono, and C. Mencar, "Subtractive clustering for seeding non-negative matrix factorizations," *Information Sciences*, vol. 257, pp. 369–387, 2014.
- [18] O. S. Alshabrawy, M. Ghoneim, W. Awad, and A. E. Hassanien, "Underdetermined blind source separation based on fuzzy c-means and semi-nonnegative matrix factorization," in *2012 Federated Conference on Computer Science and Information Systems (FedCSIS)*. IEEE, 2012, pp. 695–700.
- [19] S. M. Atif, S. Qazi, and N. Gillis, "Improved svd-based initialization for nonnegative matrix factorization using low-rank correction," *Pattern Recognition Letters*, vol. 122, pp. 53–59, 2019.
- [20] A. Yuan, M. You, D. He, and X. Li, "Convex non-negative matrix factorization with adaptive graph for unsupervised feature selection," *IEEE Transactions on cybernetics*, vol. 52, no. 6, pp. 5522–5534, 2020.
- [21] Q. Huang, X. Yin, S. Chen, Y. Wang, and B. Chen, "Robust nonnegative matrix factorization with structure regularization," *Neurocomputing*, vol. 412, pp. 72–90, 2020.
- [22] T. Ince and N. Dobigeon, "Weighted residual nmf with spatial regularization for hyperspectral unmixing," *IEEE Geoscience and Remote Sensing Letters*, vol. 19, pp. 1–5, 2022.
- [23] C.-N. Jiao, Y.-L. Gao, N. Yu, J.-X. Liu, and L.-Y. Qi, "Hyper-graph regularized constrained nmf for selecting differentially expressed genes and tumor classification," *IEEE journal of biomedical and health informatics*, vol. 24, no. 10, pp. 3002–3011, 2020.
- [24] P. Deng, T. Li, H. Wang, D. Wang, S.-J. Horng, and R. Liu, "Graph regularized sparse non-negative matrix factorization for clustering," *IEEE Transactions on Computational Social Systems*, 2022.
- [25] C. L. Lawson and R. J. Hanson, *Solving least squares problems*. SIAM, 1995.
- [26] R. Bro and S. De Jong, "A fast non-negativity-constrained least squares algorithm," *Journal of Chemometrics: A Journal of the Chemometrics Society*, vol. 11, no. 5, pp. 393–401, 1997.
- [27] A. Cichocki and A.-H. Phan, "Fast local algorithms for large scale nonnegative matrix and tensor factorizations," *IEICE transactions on fundamentals of electronics, communications and computer sciences*, vol. 92, no. 3, pp. 708–721, 2009.
- [28] N. Gillis and F. Glineur, "Accelerated multiplicative updates and hierarchical als algorithms for nonnegative matrix factorization," *Neural computation*, vol. 24, no. 4, pp. 1085–1105, 2012.